Journal of Applied Biomedicine

Original research article

False aneurysms of the thoracic aorta: anastomosis investigation using the inflation-extension test

Sandra Rečičárová [1, 2] *, Hynek Chlup [3], Michael Jonák [1], Ivan Netuka [1]

[1] *Institute for Clinical and Experimental Medicine (IKEM), Department of Cardiovascular Surgery, Prague, Czech Republic*
[2] *Charles University, First Faculty of Medicine, Prague, Czech Republic*
[3] *Czech Technical University, Faculty of Mechanical Engineering, Laboratory of Cardiovascular Biomechanics, Prague, Czech Republic*

Abstract
Introduction: False aneurysms in the thoracic aorta are dangerous complications that can occur after cardiac surgery. They often result in high mortality rates. These aneurysms are caused by damage to all layers of the aortic wall. This study aimed to pinpoint the area of the experimental specimen (native vessel, anastomosis, or prosthetic graft) with the greatest deformation, to determine whether a false aneurysm is likely to develop in the anastomotic portion.
Methods: We conducted the inflation-extension test by performing eight cycles ranging from 0 to 20. The pressure sampling frequency was 100 Hz, and each cycle lasted approximately 34 seconds, resulting in a loading frequency of 0.03 Hz. During the experiment, each camera captured 3,000 frames. Based on the data collected, we evaluated and compared the loading stages of cycle 1 and cycle 8.
Results and discussion: During loading, the native vessel experienced a dominant deformation of approximately 7% in the circumferential direction. The prosthetic graft, which had a longitudinal construction, deformed by approximately 8% in the axial direction. The prosthetic graft, on the other hand, only experienced a deformation of up to 1.5% in the circumferential direction, which was about 5 times smaller than the deformation of the native vessel. The anastomosis area was very stiff and showed minimal deformation. Additionally, there was little difference in the mechanical response between the first C1 and the eighth C8 cycle.
Conclusion: Based on the available evidence, it can be inferred that aortic false aneurysms are more likely to form just behind the suture lines in the native aorta, which is more elastic compared to stiff sections of anastomosis and prosthetic graft. Numerous pulsations of the native vessel will likely cause the impairment of the aorta at the margin of the anastomosis. This will lead to disruption of the aortic wall and false aneurysm formation in the native vessel near the area of anastomosis.

Keywords: Aortic pseudoaneurysm; The inflation-extension test; Thoracic aortic false aneurysm

Highlights:
- False aneurysms in the thoracic aorta can be a life-threatening complication following cardiac surgery and are often associated with high mortality rates.
- A test was conducted to measure inflation-extension on the experimental specimen, which included the native vessel, anastomosis, and prosthetic graft.
- The prosthetic graft underwent only 1/5th of the deformation that occurred in the native vessel. The anastomosis area was very rigid and hardly deformed at all.
- Based on the available evidence, it can be inferred that aortic false aneurysms are more likely to form just behind the suture lines in the native aorta, which is more elastic compared to stiff sections of anastomosis and prosthetic graft.

Abbreviations:
A – anastomosis; C – cycle; d – deformed mean diameter; D – mean diameter; De – outer diameter; G – prosthetic graft; H – wall thickness; l – deformed length between markers; L – reference length between markers; p – pressure; ROI – a region of interest; TAFA – thoracic aortic false aneurysm; V – native vessel

Introduction

A thoracic aortic false aneurysm (TAFA), also known as an aortic pseudoaneurysm, results from transmural disruption of the aortic wall, with the leak contained by surrounding mediastinal structures. If the aneurysm were not surrounded by these structures, it could result in fatal hemorrhaging. Rupture of the aortic wall typically occurs when all histological layers disintegrate, resulting in a false aneurysm lacking normal aortic layers (Erbal et al., 2014; Katsumata et al., 2000). The growth and expansion of TAFA are unpredictable and can cause com-

* **Corresponding author:** Sandra Rečičárová, IKEM, Department of Cardiovascular Surgery, Vídeňská 1958/9, 140 00 Prague, Czech Republic; e-mail: sandrarecicarova@yahoo.com
http://doi.org/10.32725/jab.2023.023
Submitted: 2023-06-20 • Accepted: 2023-11-24 • Prepublished online: 2023-12-13
J Appl Biomed 21/4: 174–179 • EISSN 1214-0287 • ISSN 1214-021X

pression or invasion of surrounding structures (Malvindi et al., 2010).

In 90% of cases, the patients had undergone previous surgery on their aorta or heart, such as the Bentall procedure (which accounted for 24% of cases), aortic or valve replacement or repair, coronary bypass graft, or heart transplant. A quarter of TAFA cases were caused by inflammation (Aebert and Birnbaum, 2003), 2% of patients had no known risk factors (Atik et al., 2006), 1.4% were due to complications from blunt chest trauma (Dumont et al., 2004), and the remaining cases were linked to autoimmune disease (Sullivan et al., 1988) or mycotic false aneurysms (Villavicencio et al., 2006).

In cases of TAFA, there can be anastomoses in different areas such as the proximal or distal aortic anastomosis (30%), reimplantation sites of the coronary (8%), cannulation of the vessel (4%), or other defects in the layers of the aortic wall that can lead to a poor healing process (Malvindi et al., 2010, 2013). Usually, the anastomotic sites are treated with biological glue, which stiffens the area significantly. Patients with this condition are usually asymptomatic (Mohammadi et al., 2005), but some may experience dyspnea (22%), chest pain (18%), or fever and sepsis (17%) (Razzouk et al., 1993).

When dealing with aortic false aneurysms, there are two main treatment options. Open surgery can be performed, or endovascular techniques can be utilized in certain cases. The methods used for surgical treatment vary depending on the size and location of the false aneurysm (Langanay et al., 2002). These methods can include repairing with a Dacron graft, utilizing a pericardial patch, or using direct suture repairs. For patients with small, stable TAFA, conservative treatment may be an option (Huang et al., 2006). This may also be the case for those who are unsuitable for reoperation or endovascular repair, or those who refuse surgery (Dumont et al., 2004).

The mortality rate for surgical repair of TAFA in hospitals falls between 6% and 41%, while the survival rates after surgery are 94%, 79%, and 68% at 1, 5, and 10 years, respectively. It is universally agreed by all authors that each patient should be evaluated by a team of heart experts, and that treatment must be customized to their individual needs (Atik et al., 2006; Katsumata et al., 2000).

This experimental study aimed to determine the location of the largest deformation in a specimen consisting of a native vessel, an anastomosis, and a prosthetic graft. This information will help identify if a false aneurysm is likely to occur in the anastomotic area.

Materials and methods

Mechanical tests

The experimental specimen, native vessel (V) – anastomosis (A) – prosthetic graft (G), was investigated using the inflation-extension test (Fig. 1). Using a pulsator, the sample was cyclically loaded with internal fluid pressure up to about 20 kPa, *i.e.*, 150 mmHg (Fig. 2).

The aortic tissue was retrieved from laboratory pigs (60 kg) after other unrelated animal experiments were terminated to abide by the rule of reduction of the number of experimental animals. This animal study protocol was approved by the Ministry of Health of the Czech Republic (protocol code: 14/2021, MZDR 5871/2021-4/OVZ; date of approval: February 12, 2021) and the Institutional Review Board of the Institute for Clinical and Experimental Medicine, Prague, Czech Republic (protocol code: 406; date of approval: March 3, 2021).

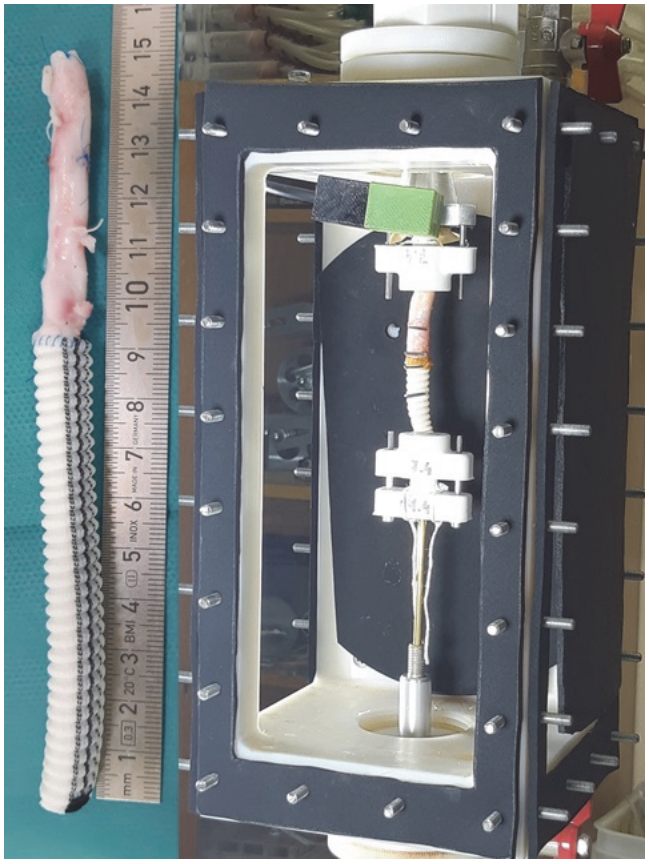

Fig. 1. The experimental specimen, native vessel (V) – anastomosis (A) – prosthetic graft (G), was investigated using the inflation-extension test

The Prolene 6-0 sutures in the anastomosis were spaced 1.33 ± 0.31 mm apart. The sutures were sealed with tissue glue Bioglue as in the surgical procedure. A very thin lubricated latex tube was inserted into the specimen. The insert was larger in diameter and length than the test specimen. The wall thickness was approximately 0.06 mm. The liner only transferred the pressure of the fluid to the specimen wall and prevented the fluid from leaking through the specimen wall. It did not affect the mechanical response.

The sample was mounted vertically in the experimental chamber. At the top, it was fixed in a fixed clamp where a Cressto KTS pressure sensor with a range of up to 28 kPa was integrated. At the bottom, it was fixed in a clamp with vertical guidance. The bottom sample reader was free to move up, down, and rotate around the vertical axis (Fig. 2). Eight cycles of 0 to 20 kPa (0 to 150 mmHg) were performed. The first seven cycles are taken as preconditioning of the specimen to stabilize the mechanical response. In this way, soft biological tissues or their substitutes, *i.e.*, arteries, veins, pericardium, valves, tendons, are tested. The sample was installed in front of the contrast background in the experimental chamber. Black markers were applied in each section of the specimen, *i.e.*, native vessel, anastomosis, and prosthetic graft (Fig. 3). The markers were fixed to the sample surface throughout the experiment. The specimen was imaged with two cameras perpendicular to each other (Fig. 2). The imaged area was approximately 52 × 37 mm (1500 × 1000 px) (Fig. 3). The resolution was 1 px = 0.035 mm. The acquired grayscale images were converted to binary maps.

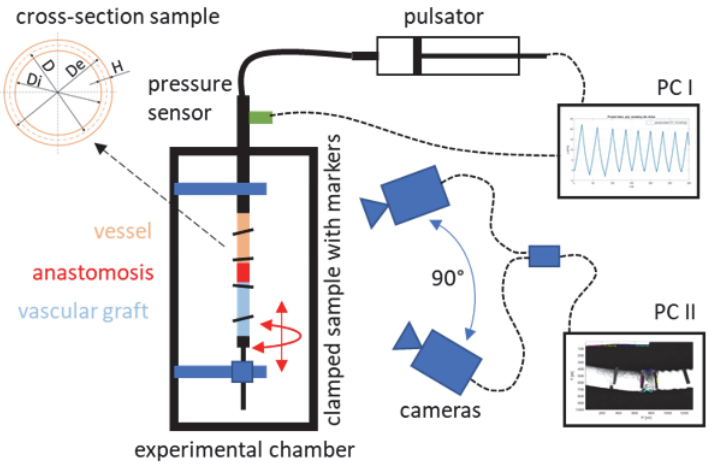

Fig. 2. Schematic of the configuration of the inflation-extension experiment with the specimen set up in the experimental chamber and specimen diameters marked in the cross-section

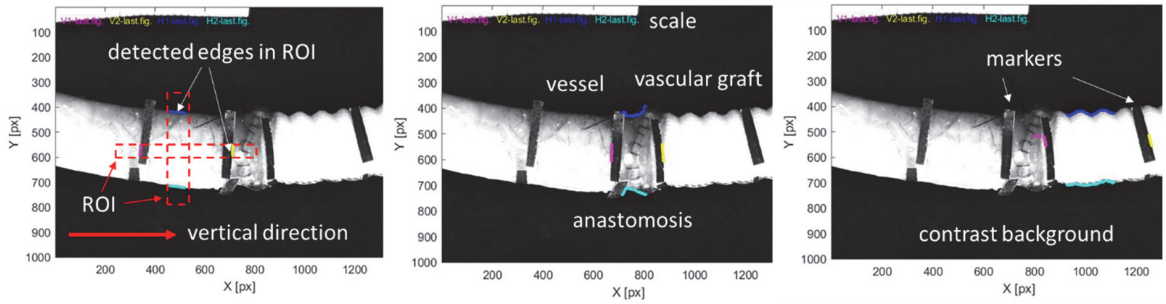

Fig. 3. Experimental specimen with installed markers for each section. The detected edges from which the deformations were calculated are indicated in color. Left – ROIs (region of interest) for the detection of horizontal (contours) and vertical (markers) edges are marked.

The pressure sampling frequency was 100 Hz. The sampling rate of the cameras was 10 fps. The internal pressure loading was quasi-static. The period of one cycle was about 34 s. The loading frequency was then about 0.03 Hz. This corresponds to about 1.8 bpm. Each camera produced 3,000 frames.

From the images in the reference configuration of each camera, the outer diameter De was measured along the length for each section at 5 locations. Means and standard deviations were calculated as shown in Table 1. A Filetta caliper micrometer was used to measure the wall thickness H with the contact force adjusted to 0.5 N. For each section, H was measured at 5 different locations around the circumference of the section. The mean diameter D was used to calculate the stress which was obtained for stress calculation. Table 1 shows the values of wall thickness H, outer diameter De, and mean diameter D as the average of the measurements from the two cameras (Table 1 and Fig. 2). Table 2 demonstrates the values of wall thickness H, outer diameter De, and mean diameter D as the average of the measurements from the two cameras.

Table 1. Values of outer De and mean D diameter of the sections of the experimental sample from each camera, and video extensometer, for the calculation of circumferential deformations and stresses, see Fig. 2 and equations (Fig. 4a) and (Fig. 4c)

	De [mm]		D [mm]	
	cam 1	cam 2	cam 1	cam 2
vessel (V)	10.07 ± 0.286	10.49 ± 0.135	8.772 ± 0.286	9.186 ± 0.135
anastomosis (A)	10.81 ± 0.484	11.15 ± 0.385	9.114 ± 0.484	9.461 ± 0.385
vascular graft (G)	9.904 ± 0.713	9.953 ± 0.751	9.51 ± 0.713	9.559 ± 0.751

Table 2. The geometry of the sections of the experimental specimen averaged from both video extensometers, where De – outer diameter, D – mean diameter, H – wall thickness, according to the scheme in Fig. 2

	De [mm]	D [mm]	H [mm]
vessel (V)	10.28 ± 0.305	8.979 ± 0.305	1.303 ± 0.303
anastomosis (A)	10.98 ± 0.47	9.287 ± 0.47	1.693 ± 0.055
vascular graft (G)	9.94 ± 0.73	9.546 ± 0.73	0.394 ± 0.02

From the acquired images, marker edges and sample contours were detected at each time point (*i.e.*, each image) in the selected ROI (region of interest) using a Matlab script (Fig. 3). From the displacements of the sample contours and markers, the values of circumferential ε_c and axial deformation ε_a (Fig. 4a and Fig. 4b) were calculated for each camera according to (Fig. 4a) and (Fig. 4b), where De – reference external diameter, de – deformed external diameter, L – reference length between markers, l – deformed length between markers. The detected edges of contours and markers were not parallel; thus, we reached the subpixel level of resolution.

$$\varepsilon_c = \frac{de - De}{De} \qquad \text{(a)}$$

$$\varepsilon_a = \frac{l - L}{L} \qquad \text{(b)}$$

$$\sigma_c = p\frac{(d/2)^2 l}{(D/2)HL} \qquad \text{(c)}$$

$$\sigma_a = \sigma_c/2 \qquad \text{(d)}$$

Fig. 4. Math formulae

Blood vessel samples are usually not deformed as ideal cylindrical tubes of circular cross-sections. The obtained strain values from two synchronously running cameras (two directions) were averaged. The resulting strain values were phased with the pressure values. The native vessel, prosthetic graft, and anastomosis have different basic geometry, *i.e.*, different wall thicknesses and diameters (Table 1 and 2). The cross-sections of the pressure transmitting wall are different, and hence different strains are generated in the wall. The effect of the different cross sections is eliminated in the stress calculation. The stresses in the circumferential σ_c and axial (longitudinal) direction σ_a were calculated according to the relations for thin-walled cylindrical shells (Fig. 4c) and (Fig. 4d) considering the incompressibility of the materials, where p – pressure, D – reference mean diameter, d – deformed mean diameter, and H – wall thickness. From the experimental data, the loading part of 1 (C1) and 8 (C8) cycles were evaluated and compared. We are primarily interested in the mechanical response during the eighth cycle, C8. This procedure was applied to each section of the specimen, see Fig. 5a, b and Fig. 6.

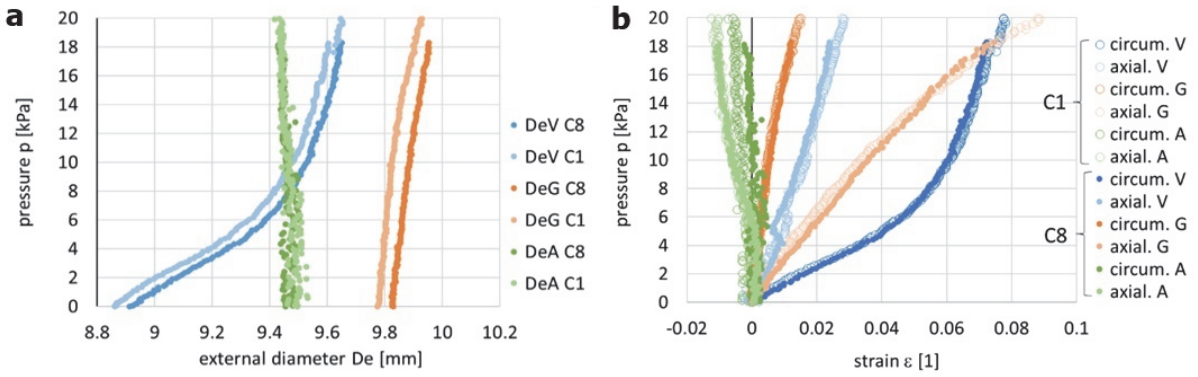

Fig. 5. (**a**) Experimental characteristics of pressure-external diameter De for monitored sections (V-vessel, A-anastomosis, G-graft), loading parts 1 and 8 of the cycle. (**b**) Experimental pressure-strain characteristics in circumferential and axial directions for the monitored sections of the specimen (native vessel – anastomosis – prosthetic graft) in the first and the eighth loading cycle.

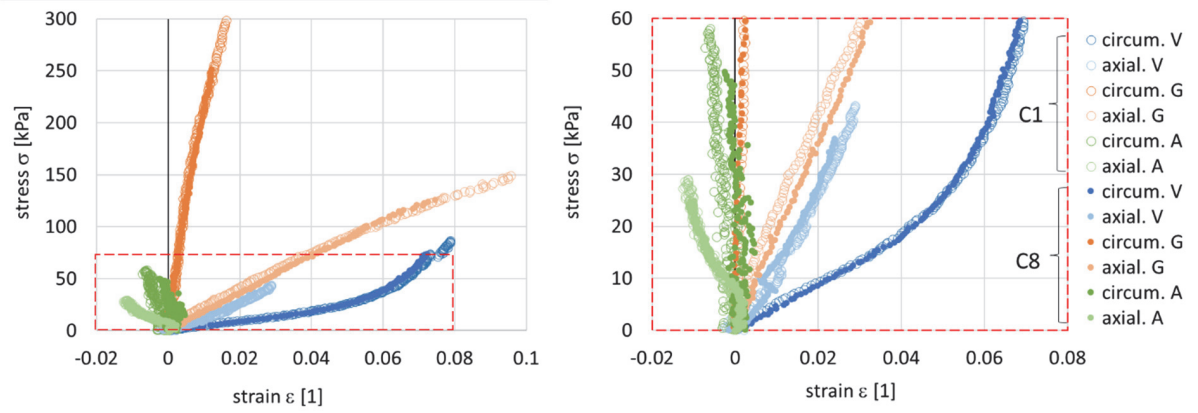

Fig. 6. Stress-strain characteristics in the circumferential and axial directions for the tested specimen sections (native vessel – anastomosis – prosthetic graft) in the first and eighth loading cycle. Right – detail of the region marked by the dashed red line.

Results and discussion

In the obtained characteristics of pressure-De, pressure-strain, and especially stress-strain we are interested in the slope of the characteristics (see Fig. 5a, b, and Fig. 6). The characteristics of the native vessel have, as expected, a typical nonlinear course, convex character, and blue curves. As the load increases, the material stiffens, *i.e.*, the slope of the characteristics is steeper. As the deformation of the artery wall increases, it creates more resistance. The opposite is true for a prosthetic graft. The mechanical response has a slightly concave character and orange curves, similar to artificial polymer materials. The characteristic can be considered linear in the physiological pressure range up to 16 kPa (120 mmHg). The mechanical response of the anastomosis has a linear character and green curves.

The largest changes in the monitored outer diameter De were detected in the native vessel (Fig. 5a). There was very little change in the outer diameter of the prosthetic graft. In the anastomosis area, De hardly changed (Fig. 5a). From the changes in the outer diameter De, circumferential deformations were calculated according to corresponding math formulae (Fig. 4a). The dependencies of the pressure and stress in the specimen wall on the deformations are shown in Fig. 5b and Fig. 6. Details of the anastomosis section are shown in Fig. 7. In the circumferential direction, the native vessel deformed the most, up to about 7% (ε = 0.07). In the axial direction, it was up to approximately 3%, see Fig. 5b and Fig. 6. The prosthetic graft achieved deformations of approximately 1.5% in the circumferential direction and 8% in the axial direction. The prosthetic graft achieved smaller deformations in the circumferential direction than in the axial direction. This is the reverse of the native vessel. The native vessel deforms more in the circumferential direction than in the axial direction. This phenomenon is probably due to the longitudinal constriction of the prosthetic graft. Physiologically, circumferential compliance, *i.e.*, deformation in the circumferential direction, is essential. The tested prosthetic graft is stiffer in the circumferential direction than the native vessel (Fig. 5b and Fig. 6). The anastomosis region was the least compliant. This was to be expected. In the circumferential direction, it is hardly deformed. In the axial direction, the anastomosis section is shortened by 1% (Fig. 7). The native vessel and the prosthetic graft can be considered anisotropic material. In the circumferential and axial directions, they deform differently under load (Fig. 6). In the anastomosis region, it is not so clear. The data obtained are more scattered (Fig. 7).

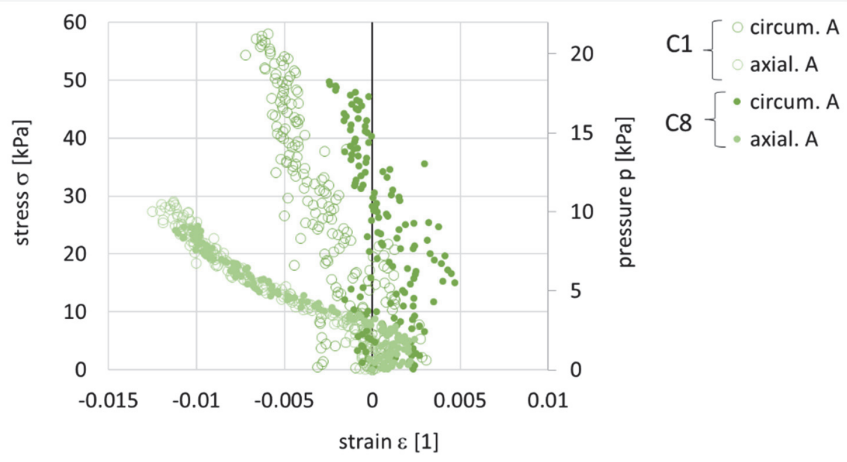

Fig. 7. Detail of the mechanical response of the anastomosis section

The stiffness in the circumferential direction may affect physiological functionality and hemodynamic conditions, *e.g.*, pulse wave transmission.

The difference between the mechanical response of 1 and 8 cycles was very small. The characteristics of C1 and C8 lie very close to each other. For the native vessel, the characteristics at higher strains for C8 are slightly steeper (Fig. 5b and Fig. 6). The material stiffens slightly due to cyclic loading. This is as expected. The reverse trend is shown by the prosthetic graft. The anastomosis area deformed very little. Thus, proportionally, the change in mechanical response for C1 and C8 is more pronounced in the circumferential direction (Fig. 7). In the axial direction, it is the same.

A literature review on inflation-extension tests revealed that there have been experiments using native aorta. However, there have been no published tests on anastomosis (Kim and Baek, 2011; Sommer et al., 2018; Tarraf et al., 2023; Veljković et al., 2014). Our specimen, *i.e.*, the native vessel-anastomosis-prosthetic graft, was cyclically loaded with internal pressure using the inflation-extension test. The experimental characteristics of pressure-external diameter De, pressure-strain, and stress-strain were obtained. There was minimal difference between the mechanical response at the first C1 and the eighth C8 cycle. As expected, an anisotropic nonlinear material response was observed for the native vessel and the prosthetic graft. It has been found that the isotropic model overestimates values of stresses in the axial, and underestimates values of stresses in the circumferential direction of artery segment, due to pronounced tissue anisotropy (Veljković et al., 2014).

The native vessel deformed dominantly in the circumferential direction, approximately 7%, during loading and 3% in the axial direction. This conclusion aligns with the findings of other authors (Sommer et al., 2018; Tarraf et al., 2023). We did not note any variation in stiffness between the anterior and posterior regions. However, a different experiment found that the stiffness of the posterior region was significantly greater than that of the anterior region (Kim and Baek, 2011).

Probably due to longitudinal construction, the prosthetic graft deformed in the axial direction, approximately 8%. In the circumferential direction, the deformation of the prosthetic graft was only up to 1.5%, *i.e.*, the deformation was approximately 5 times smaller than that of the native vessel. The anastomosis area was very stiff. The section of anastomosis was almost not deformed. At a maximum internal pressure load of 20 kPa (150 mmHg), the dominant axial deformation was up to –1%. This means that the anastomosis area was only slightly shortened. In engineering practice, the initiation of failure tends to be at the point of step changes in material stiffness, *e.g.*, the point of onset of crack propagation.

Conclusion

We cyclically loaded the native vessel-anastomosis-prosthetic graft with internal pressure using the inflation-extension test to determine whether a false aneurysm is likely to develop in the anastomotic portion. During loading, the native vessel experienced a dominant deformation of approximately 7% in the circumferential direction. The prosthetic graft, which had a longitudinal construction, deformed by approximately 8% in the axial direction. On the other hand, the prosthetic graft only experienced a deformation of up to 1.5% in the circumferential direction, which was about 5 times smaller than the deformation of the native vessel. The anastomosis area was very stiff and showed minimal deformation.

Based on the available evidence, it can be inferred that aortic false aneurysms are more likely to form just behind the suture lines in the native aorta, which is more elastic compared to stiff sections of anastomosis and prosthetic graft. Numerous pulsations of the native vessel will likely cause the impairment of the aorta at the margin of the anastomosis. This will lead to disruption of the aortic wall and false aneurysm formation in the native vessel near the anastomosis area.

Acknowledgments
We would like to thank Jaroslav Chlupac for providing porcine aortic tissues.

Ethical aspects and conflict of interest
The authors have no conflict of interest to declare.

Funding
Supported by Ministry of Health, Czech Republic – conceptual development of research organization (“Institute for Clinical and Experimental Medicine – IKEM, IN 00023001”).

References

Aebert H, Birnbaum DE (2003). Tuberculous pseudoaneurysms of the aortic arch. J Thorac Cardiovasc Surg 125(2): 411–412. DOI: 0.1067/mtc.2003.130.

Atik FA, Navia JL, Svensson LG, Vega PR, Feng J, Brizzio ME, et al. (2006). Surgical treatment of pseudoaneurysm of the thoracic aorta. J Thorac Cardiovasc Surg 132(2): 379–385. DOI: 10.1016/j.jtcvs.2006.03.052.

Dumont E, Carrier M, Cartier R, Pellerin M, Poirier N, Bouchard D, Perrault LP (2004). Repair of aortic false aneurysm using deep hypothermia and circulatory arrest. Ann Thorac Surg 78(1): 117–120; discussion 120–121. DOI: 10.1016/j.athoracsur.2004.01.028.

Erbel R, Aboyans V, Boileau C, Bossone E, di Bartolomeo RD, Eggebrecht H, et al. (2014). 2014 ESC Guidelines on the diagnosis and treatment of aortic diseases: Document covering acute and chronic aortic diseases of the thoracic and abdominal aorta of the adult. The Task Force for the Diagnosis and Treatment of Aortic Diseases of the European Society of Cardiology (ESC). Eur Heart J 35(41): 2873–2926. DOI: 10.1093/eurheartj/ehu281.

Huang LJ, Yu FC, Sun LZ, Tian LX, Chu JM, Lü JH, et al. (2006). Treatment of aortic pseudoaneurysm with interventional procedure. Chin Med J (Engl) 119(7): 612–616.

Katsumata T, Moorjani N, Vaccari G, Westaby S (2000). Mediastinal false aneurysm after thoracic aortic surgery. Ann Thorac Surg 70(2): 547–552. DOI: 10.1016/s0003-4975(00)01300-x.

Kim J, Baek S (2011). Circumferential variations of mechanical behavior of the porcine thoracic aorta during the inflation test. J Biomech 44(10): 1941–1947. DOI: 10.1016/j.jbiomech.2011.04.022.

Langanay T, Verhoye JP, Corbineau H, Agnino A, Derieux T, Menestret P, et al. (2002). Surgical treatment of acute traumatic rupture of the thoracic aorta a timing reappraisal? Eur J Cardiothorac Surg 21(2): 282–287. DOI: 10.1016/s1010-7940(01)01133-2.

Malvindi PG, Cappai A, Raffa GM, Barbone A, Basciu A, Citterio E, et al. (2013). Analysis of postsurgical aortic false aneurysm in 27 patients. Tex Heart Inst J 40(3): 274–280.

Malvindi PG, van Putte BP, Heijmen RH, Schepens MA, Morshuis WJ (2010). Reoperations for aortic false aneurysms after cardiac surgery. Ann Thorac Surg 90(5): 1437–1443. DOI: 10.1016/j.athoracsur.2010.06.103.

Mohammadi S, Bonnet N, Leprince P, Kolsi M, Rama A, Pavie A, Gandjbakhch I (2005). Reoperation for false aneurysm of the ascending aorta after its prosthetic replacement: surgical strategy. Ann Thorac Surg 79(1): 147–152; discussion 152. DOI: 10.1016/j.athoracsur.2004.06.032.

Razzouk A, Gundry S, Wang N, Heyner R, Sciolaro C, Van Arsdell G, et al. (1993). Pseudoaneurysms of the aorta after cardiac surgery or chest trauma. Am Surg 59(12): 818–823.

Sommer G, Benedikt C, Niestrawska JA, Hohenberger G, Viertler C, Regitnig P, et al. (2018). Mechanical response of human subclavian and iliac arteries to extension, inflation and torsion. Acta Biomater 75: 235–252. DOI: 10.1016/j.actbio.2018.05.043.

Sullivan KL, Steiner RM, Smullens SN, Griska L, Meister SG (1988). Pseudoaneurysm of the ascending aorta following cardiac surgery. Chest 93(1): 138–143. DOI: 10.1378/chest.93.1.138.

Tarraf SA, Kramer B, Vianna E, Gillespie C, Germano E, Emerton KB, et al. (2023). Lengthwise regional mechanics of the human aneurysmal ascending thoracic aorta. Acta Biomater 162: 266–277. DOI: 10.1016/j.actbio.2023.03.023.

Veljković DŽ, Ranković VJ, Pantović SB, Rosić MA, Kojić MR (2014). Hyperelastic behavior of porcine aorta segment under extension-inflation tests fitted with various phenomenological models. Acta Bioeng Biomech 16(3): 37–45.

Villavicencio MA, Orszulak TA, Sundt TM 3rd, Daly RC, Dearani JA, McGregor CG, et al. (2006). Thoracic aorta false aneurysm: what surgical strategy should be recommended? Ann Thorac Surg 82(1): 81–89; discussion 89. DOI: 10.1016/j.athoracsur.2006.02.081.